DEVELOPMENT OF A MULTI-DIMENSIONAL CLEANING SIEVE TO OPTIMIZE THRESHED OUTPUTS DISTRIBUTION AND EXPERIMENTS IN COMBINE HARVESTER
/
联合收获机多维均布清选装置开发与试验

Xiaoyu CHAI[1)], Pengtao ZHANG[1)], Xinting LIU[2)], Lizhang XU[1)], Liyuan CHEN[1*)], Qiang LI[3)] and Longhai WANG[4)]
[1)] School of Agricultural Engineering, Jiangsu University, Zhenjiang, 212013, Jiangsu, China;
[2)] Weichai Lovol Intelligent Agricultural Technology Co. Ltd, Weifang, 261000, Shangdong, China;
[3)] Tongzhou District Agricultural Mechanization Technology Extension Station, Nantong, 226300, Jiangsu, China;
[4)] Institute of Process Equipment, College of Energy Engineering, Zhejiang University, Hangzhou, 310027, Zhejiang, China.
*Corresponding authors. Email: xfpaxy521123@163.com
DOI: https://doi.org/10.35633/inmateh-75-85

***Keywords:** multidimensional cleaning method; rapeseed; CFD-DEM; combined harvester*

ABSTRACT
Searching for and identifying methods to reduce grain cleaning loss, grain impurity, and improve cleaning efficiency is crucial for processing threshed rapeseed outputs in uneven conditions. Leveling a single-degree-of-freedom cleaning sieve becomes particularly challenging under terrain undulations and limited cleaning space. Based on spiral theory and mechanical design principles, this study explores a multi-degree-of-freedom cleaning sieve capable of vertical movement along the horizontal plane and rotation around its center. This design allows the sieve to adjust its relative angle, enabling a more uniform distribution of threshed outputs. A CFD-DEM coupling method was used to simulate the movement of these outputs. The cleaning sieve inclined forward and to the right served as the experimental group, while a horizontal cleaning sieve functioned as the control group. Compared to the control, the experimental group showed a 14.6% reduction in grain loss and a 2.3% decrease in impurities. Furthermore, the centroid motion of the rapeseed was enhanced prior to sieving, facilitating more effective separation, while the movement speed of impurities outside the cleaning shoe increased, aiding impurity removal.

摘要
针对丘陵地区地形起伏，小型收获机清选空间有限的难题，多自由度的清选装置开发是相当具有挑战性的。文章基于螺旋理论和机械设计方法，探索了一种可以在水平方向上垂直移动并绕其中心旋转的多自由度清选筛。该清选筛通过调整筛面角度实现脱出物均布，实现清选性能和清选效率的提升。基于 CFD-DEM 耦合方法模拟脱出物运动，将清选筛前倾和向右倾斜状态设置为实验组，清选筛水平状态设置为对照组。结果表明，对比对照组，试验组籽粒损失和含杂分别减少了 14.6% 和 2.3%。同时，在筛分前，油菜籽、杂质的质心运动速度明显增强，这有利于去除含杂和提高筛分效率。该研究方法对于收获装备转型升级具有重要的实际意义。

INTRODUCTION
Rapeseed is the largest source of edible vegetable oil in China. Accelerating the development of rapeseed mechanization, supporting the upgrading of the oil industry, and reducing China's heavy dependence on imported raw materials for vegetable oil are among the country's most pressing priorities. Hilly and mountainous areas account for 1/3 of the country's crop cultivation area. Between the hills and low mountains there are many river valley basins. The four seasons are distinct, the land is fertile, suitable for rape planting. The primary crops of wheat and corn differ substantially in their agronomic and physical attributes compared to rapeseed *(Zhao et al, 2022; Zhang et al, 2024; Li et al, 2024)*, making it impractical to directly apply their harvesting design methods and equipment to rapeseed. Hilly and mountainous regions typically experience abundant rainfall and sufficient sunshine, leading to robust rapeseed growth. In these areas, rapeseed plants usually range from 220 mm to 250 mm in height, and the grass-to-grain ratio is significantly higher than in the plains—often reaching as much as 4–5:1. After threshing and separation, the grain volume in the rapeseed material fed into the cleaning shoe accounts for only about 8%, while the volume of impurities is considerably higher. These impurities are diverse in composition, and the small, spherical rapeseed grains are mixed with various irregular residues.

[1] Xiaoyu Chai (Lecturer), Pengtao Zhang (M. Eng. student), Xinting Liu (Engineer), Lizhang Xu (Professor), Liyuan Chen (Doctor), Qiang Li (Engineer), Longhai Wang (Doctor).

This complex mixture makes stratification and separation difficult, resulting in a portion of the grains being discharged along with the impurities, thus increasing grain loss. Additionally, some impurities may fall into the grain auger, further raising the impurity content of the harvested product.

Unlike traditional field harvesting equipment, threshing and cleaning systems must account for variations in terrain *(Vlădut et al, 2023; Zhang et al, 2024)*. In hilly and mountainous regions, rapeseed suitable for mechanized harvesting is often cultivated on sloped lands, with inclines ranging from 6° to 15° in hilly areas and 15° to 25° on terraced slopes. For combine harvester manufacturers, incorporating components, or even designing entire machines, with the capability to adapt to uneven surface topography is essential for improving harvesting adaptability in these challenging environments. The IDEAL 10T combine harvesters *(Fendt, 2025)* are equipped with multiple guide strips and multi-layer vibrating sieves, enabling uniform material distribution during multi-crop harvesting. Technologies such as header contouring devices and 3D multi-layer vibrating sieves have been implemented *(MF, 2025; Claas, 2025)* to automatically adjust to varying slope angles, maintaining a level threshing and cleaning system. Experts and researchers have been actively engaged in developing small-scale harvesting machinery tailored for hilly and mountainous regions. To address the accumulation of threshed material on the sieve surface, caused by the topography of hilly and mountainous regions, technologies for threshed material dispersion and the analysis of particle movement trajectories have become particularly critical. A three-stage vibrating sieve equipped with guide strips and a cross-flow fan *(Case, 2025)* was employed to achieve more uniform airflow across the entire sieve, thereby improving the even distribution of materials on the sieve surface. The CFD-DEM coupling method has been increasingly applied to simulate two-phase flow performance in complex agricultural systems *(Wang et al., 2024; Shen et al., 2024; Tanneru et al., 2024)*. Korn et al. utilized this method to simulate the separation process of threshed materials within the cleaning unit of a combine harvester. The CFD-DEM coupling method has been employed to simulate the movement of jojoba and flax threshing materials within an airflow-sieve cleaning device, enabling the prediction of grain separation performance under specific design conditions *(El-Emam, 2021)*. Similarly, CFD-DEM has been used to study the movement of corn and rapeseed threshed outputs during the sieving process *(Wang et al., 2021)*, helping determine optimal parameters such as sieve hole sidewall angle, airflow velocity, and airflow direction angle. These studies demonstrate that CFD-DEM simulations are highly effective for analyzing particle motion, offering clear insights into grain dynamics. As a result, the advantages of the CFD-DEM method will be applied in this study to enhance the analysis of threshed material behavior and cleaning performance.

Based on the above, current gas-solid coupling simulations in the cleaning process typically focus only on the primary components present on the cleaning sieve. However, in real-world conditions, particularly in hilly regions, rapeseed accumulation is often severe, and traditional simulations rarely account for the accumulation state of separated materials or the complex interactions between them. Furthermore, many simulations consider only a single particle type, overlooking the uneven distribution of different particle types across various regions. This simplification results in a significant deviation from the actual separation process. Therefore, it is essential to study the movement trajectories of separated particles under conditions of inclined accumulation and to further explore the underlying sieving mechanisms in order to enhance separation performance and overall cleaning efficiency.

MATERIALS AND METHODS

Multidimensional motion theory of the cleaning device

When a combine harvester operates in hilly and mountainous terrain, changes in surface topography can cause the entire cleaning device to tilt both in the forward-backward direction and the left-right direction. Moreover, the centrifugal force acting on threshed outputs in the longitudinal axial flow threshing and separation device typically causes the threshed outputs to distribute unevenly, with higher concentrations on both sides and lower concentrations in the middle *(Liu et al, 2022; Li et al, 2022).* This uneven distribution leads to threshed output accumulation on both sides of the sieve surface, negatively affecting the sieving efficiency. Therefore, it is necessary to develop a multidimensional cleaning device that can adapt to varying terrain conditions and dynamically regulate the distribution of threshed outputs. To minimize the impact of external factors such as terrain on the cleaning device, it is essential to eliminate the influence of forward-backward and left-right tilting on the cleaning system. Let the forward direction of the combine harvester be defined as the positive x-axis. In the following descriptions, "forward," "backward," "left," "right," "up," and "down" correspond to the positive x-axis, negative x-axis, positive y-axis, negative y-axis, positive z-axis, and negative z-axis, respectively.

The designed multidimensional cleaning device compensates for the effects of terrain on the cleaning shoe in both the forward-backward and left-right directions. This device features three degrees of freedom, including rotation around the x-axis and y-axis to adjust the uneven distribution of threshed outputs in the left-right direction.

Additionally, movement along the z-axis ensures that the relative position of the sieve surface remains constant within the adjustment range when the terrain has significant vertical undulations. The primary technical specifications are detailed in Table 1.

A combination of the SPS/RPS-UP parallel stable platform and the 2PSS-U parallel stable platform was selected to achieve multidimensional adjustment of the sieve surface within the confined space. The principle diagram of the multidimensional adjustment mechanism for the sieve surface is shown in Fig. 1.

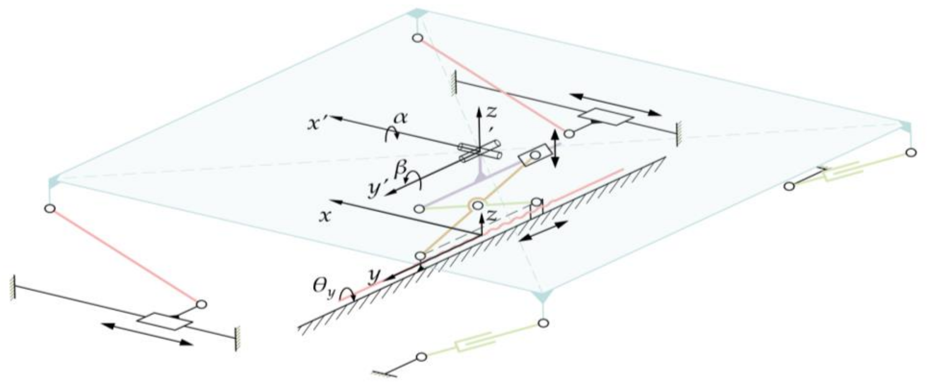

Fig.1 - Prototype of the multi-dimensional cleaning mechanism

The 2PSS-U parallel stable platform serves as the core of the design, with its U-branches modified to PU-branches. To accommodate the longitudinal movement, range of the mechanism, a retractable linear drive device is incorporated into the middle PU branch of the sieve surface. Additionally, two support points are added at the vertices of the platform to maintain dynamic stability during the adjustment process.

Table 1

Performance specifications of the multidimensional cleaning device

No.	Performance	Value	Remarks
1	Adjust the limit position around the x-axis	+8°±0.5°, -8°±0.5°	Angle with the horizontal direction
2	Adjust the limit position around the y-axis	+8°±0.5°, -8°±0.5°	Angle with respect to the horizontal direction
3	Range of longitudinal movement for the mechanism	≤65 mm	The limit position of the movement space must ensure a certain distance between the vibration plate and the fish scale sieve
4	Load capacity of the mechanism	≥2kg	Mass flow rate of the threshed outputs stream
5	Rotation angle around the x-axis	≤5°	Angle with the horizontal direction
6	Rotation angle around the y-axis	≤5°	Angle with the horizontal direction

Structural design of multi-dimensional cleaning device

The multi-dimensional cleaning device, designed to adapt to terrain variations and the distribution state of separated materials, features a perforated sieve at its output end, positioned between the fish-scale screen and the vibrating plate. The structural principle of the adjustable cleaning device is illustrated in Fig. 1, while the designed multi-dimensional cleaning device is shown in Fig. 2. The system consists of a frame, an upper platform, a screw, a screw nut, connecting rods, and sliding blocks mounted on the upper platform. To enable folding motion, connecting rods with spherical joints at both ends are installed on either side of the upper sieve surface. At the center of the sieve, an "X"-shaped retractable cross-link mechanism serves as a linear actuator. The rotation of the screw, which is arranged along the y-axis, causes the screw nut to move along the y-axis. This screw also results in changes in the angle between the cross-links, which drives the upper platform to move up and down along the z-axis. At the two rear vertices of the platform, spherical joints and damping slide rods are used for connection. The damping slide rods are moving pairs with damping characteristics, and their other ends are connected to the frame via spherical joints.

These two damping slide rods act as driven components and enhance the stability of the mechanism's movement without affecting its degrees of freedom. Forward drive slider is fixed on the power guide rail on the side wall of the cleaning shoe, with a certain gap introduced between it and the spherical joint to reduce the probability of interference with the side wall during platform movement.

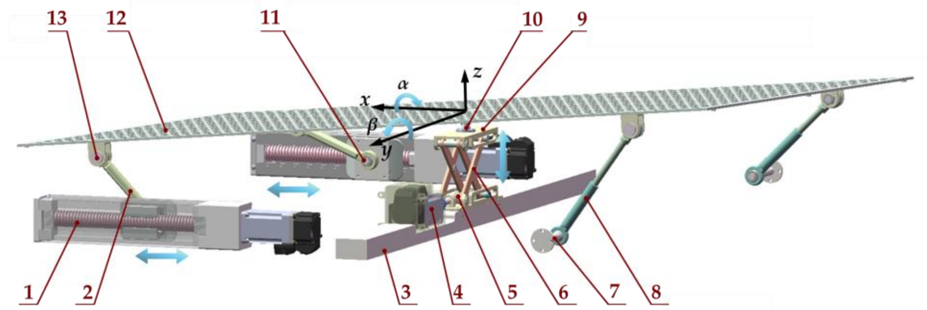

Fig. 2 - Schematic diagram of multi-dimensional cleaning device structure.
1. Screw sliding table; 2. Double spherical hinge connecting rod; 3. Support beam; 4. Lifting platform drive motor; 5. Drive screw; 6. Lifting platform connecting rod; 7. Damping rod support; 8. Damping rod; 9. Upper platform of the lifting platform; 10. Hook hinge; 11. Lower spherical hinge; 12. Movable screen surface; 13. Upper spherical hinge

The fixed end of the lifting platform is mounted to the bottom of the support beam, while its movable end is connected to the bottom of the hook joint. The center of the perforated sieve's rectangular envelope is attached to the top of the hook joint. At the four corners of the perforated sieve, four sets of positioning holes are symmetrically distributed, using the envelope's rectangular center as the origin. Four sets of positioning pins are employed to accurately position the four-fork frame bearing seats into the designated fixed holes.

The multi-degree-of-freedom sieving device is integrated into the cleaning shoe, as illustrated in Fig. 3. By combining the configurations shown in Fig. 1 and Fig. 2, a ball joint is mounted into the fork frame bearing seat of the multi-degree-of-freedom screening structure. A slider is affixed to the screw slide platform, and the central region of the slider incorporates a cylindrical structure designed to connect with the lower spherical joint. This design enables the lower spherical joint to move synchronously with the active end of the screw slide platform. The lower end of the damping rod is connected to a spherical joint on the damping rod support, while the upper end is linked to the fork frame bearing seat positioned behind the moving sieve. This configuration enables stable three-degree-of-freedom adjustment, even within the constraints of limited installation space.

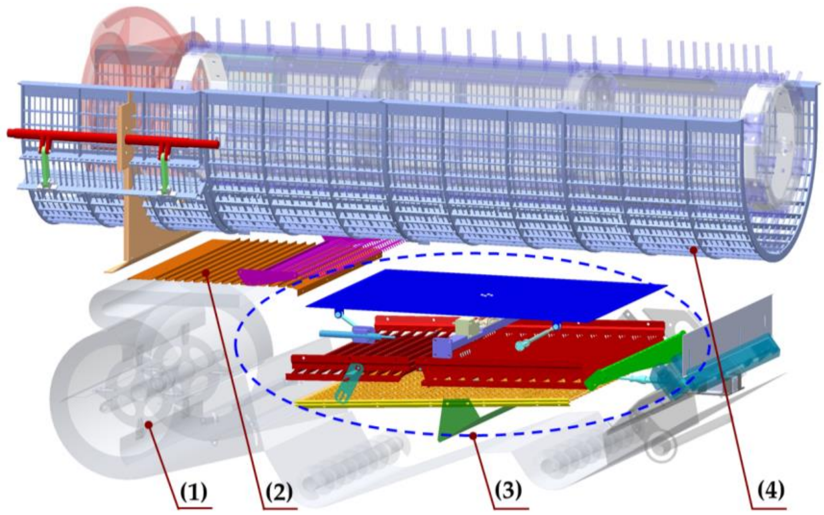

Fig. 3 -The multi-dimensional cleaning sieve in the cleaning shoe
(1) Longitudinal axial threshing cylinder; (2) Multi-dimensional perforated sieve; (3) Centrifugal fan; (4) Vibrating sieve.

Coupled simulation of threshed outputs in gas-solid two-phase flow

CFD and DEM coupled simulation model

To accurately reflect the cleaning process, it is necessary to analyze the combined effects of gas flow and vibrating sieves. In a gas-solid two-phase flow system, gas typically acts as the continuous phase, while the solid phase is dispersed as particles or clumps within the gas.

This study uses the computational fluid dynamics software Fluent (V15.0, CFD Inc., USA) to simulate the gas phase flow field, and discrete element method software EDEM (V2.7, DEM Solutions Ltd., UK) to analyze the motion and force states of solid phase particles. Through a coupling interface, CFD and DEM achieve real-time data exchange, including the transfer of mass, momentum, and energy, thus completing a bidirectional coupled numerical simulation of gas-solid two-phase flow. The advantage of this coupling technology is that it integrates the geometric characteristics of solid particles (such as shape and size) and physical properties (such as material properties and friction coefficients), providing a more accurate capture of the interactions and effects between the gas and solid phases *(Tanneru et al, 2024).*

The continuity equation and momentum equation for the gas phase can be represented as follows *(Xu et al, 2020):*

$$\frac{\partial \varepsilon \rho}{\partial t} + \nabla \cdot \rho \varepsilon u = 0 \tag{1}$$

$$\frac{\partial \varepsilon \rho}{\partial t} + \nabla \cdot \rho \varepsilon u \mu = -\nabla \rho + \nabla \cdot (\mu \varepsilon \nabla u) + \rho \varepsilon g - S \tag{2}$$

where:

ε represents the volume fraction term; ρ is the gas density, kg·m^{-3}; u is the gas velocity, m·s^{-1}; μ is the dynamic viscosity coefficient, Pa·s, and S is the momentum sink, kg·m^2·s^{-1}.

The contact model forms the core basis of the Discrete Element Method (DEM). It essentially simulates the elastic-plastic mechanical behavior of particles under quasistatic conditions when in contact. Although the contact relationships between particles are nonlinear, approximate superposition principles are often used for analysis. In EDEM software, the default contact model is the Hertz-Mindlin model, also known as the "elastic-damping-friction contact mechanics model." This model takes into account the elastic deformation, damping effects, and frictional forces between particles during contact. Hertz-Mindlin model was employed to investigate the motion behavior of rapeseed particles in a multi-airflow cleaning device, the equations can be represented as follows *(Ma et al, 2022).*

$$F_{cni} = \frac{4}{3} E^* (R^*)^{1/2} \alpha^{3/2} \tag{3}$$

$$F_{dni} = -2\sqrt{\frac{5}{6}} \beta \sqrt{S_n m^*} v_n^{rel} \tag{4}$$

$$F_{cti} = -S_t \delta \tag{5}$$

$$F_{dti} = -2\sqrt{\frac{5}{6}} \beta \sqrt{S_t m^*} v_t^{rel} \tag{6}$$

where:

F_{cni} represents the normal contact force between particles, N; E^* is the equivalent elastic modulus, Pa; R^* is the equivalent particle radius, m; α is the normal overlap between the particles. F_{dni} represents the normal damping force between particles, N; β is the coefficient; S_n is the normal stiffness, N·m^{-1}; m^* is the equivalent mass, kg; $v_{\mathrm{n}}^{\mathrm{rel}}$ is the normal component of relative velocity, m·s^{-1}. F_{cti} is the tangential contact force between particles, N; S_{t} is the tangential stiffness between the particles, N·m^{-1}; δ is the tangential overlap between the particles. F_{dti} represents the tangential damping force between particles, N; $v_{\mathrm{t}}^{\mathrm{rel}}$ is the tangential component of relative velocity, m· s^{-1}.

Fluent - EDEM Gas-Solid Coupling Simulation

Establishment of flow channel model and boundary mesh division. After preliminary research and simulation of the airflow distribution on the sieve surface, it was found that a leaning forward and leaning right condition of the multidimensional cleaning sieve is most advantageous for the selection process in a combine harvester. Therefore, this configuration was selected as the basis for particle analysis and designated as the experimental group, while the condition with a horizontal sieve surface served as the control group. The Fluent-EDEM digital simulation method was employed to compare the movement of rapeseed threshed outputs under the influence of terrain and the movement of the threshing drum. The coupled flow path model of the experimental group is illustrated in Fig. 4.

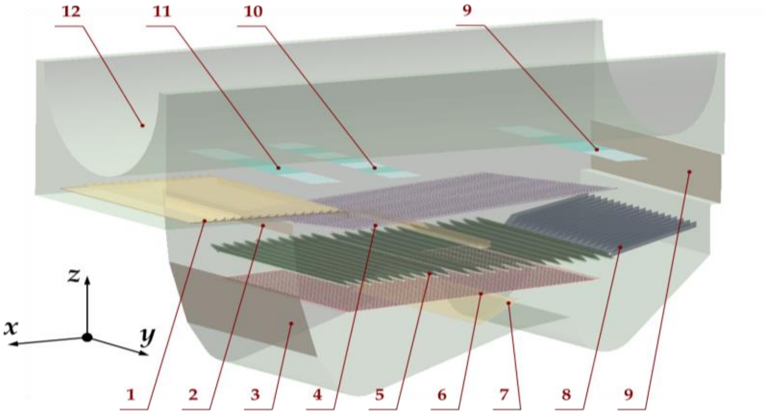

Fig. 4 - Coupled flow channel model of the cleaning shoe

1. Shaking plate; 2. Upper inlet; 3. Lower inlet; 4. Adjustable perforated sieve; 5. Fish scale sieve; 6. Woven sieve; 7. Guiding plate; 8. Tail sieve; 9. Outlet; 10. Threshing drum; 11. Concave sieve; 12. Particle factory ①~③; 13. Particle factory ④~⑩; 14. Particle Factory ⑪~⑬.

The flow path model was designed with an arcuate structure for the perforated plate sieve to facilitate observation of grain movement. The model includes upper and lower air inlets representing the fan's air outlets, with the airflow speed set to the average speed of the section. The meshing software was used to create a tetrahedral mesh for the cleaning shoe flow path model, resulting in a total of 6,021,268 mesh elements. The mesh file was saved as an MSH file and imported into both Fluent and EDEM software for simulation.

Establishment of EDEM environment and particle model. An experiment was conducted to observe the distribution pattern of the threshed outputs under the longitudinal axial threshing drum. This involved uniformly arranging 70 collection boxes, each with dimensions of 110×190×110 mm³, beneath the Longitudinal axial threshing drum, as illustrated in Fig. 5. In the EDEM software simulation, it is necessary to model the simulation objects. Therefore, the components of the output materials need to be categorized. The threshed output samples, collected from beneath the longitudinal axial-flow threshing device (as shown in Fig. 5), were manually sieved to identify four main types of threshed output components, as illustrated in Fig. 6.

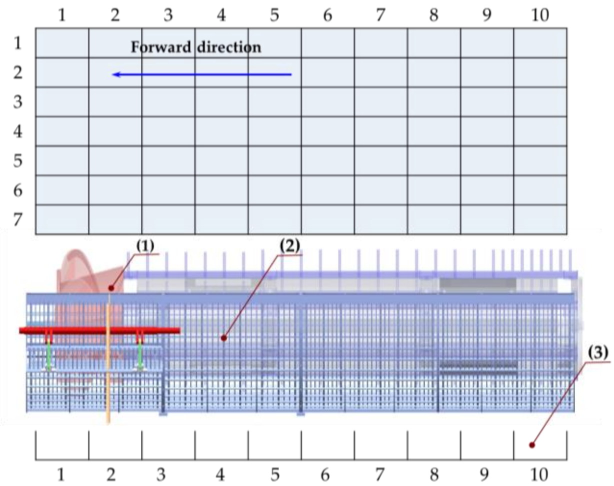

Fig. 5 - Longitudinal axial threshing drum and receiving box placement position

(1) Longitudinal axial threshing drum; (2) Concave sieve; (3) Receiving box.

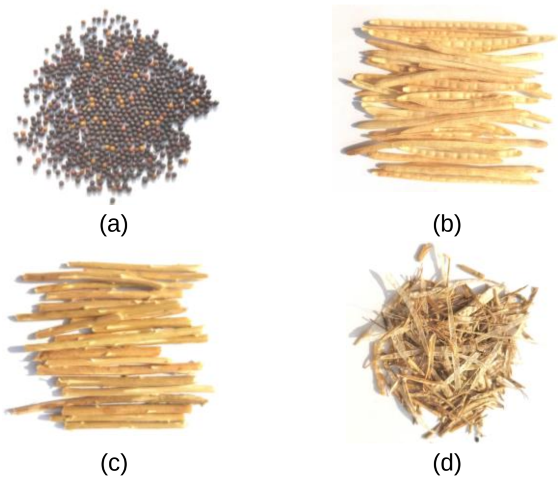

Fig. 6 - Main components of the rapeseed threshed outputs

(a) Rapeseeds; (b) Pod shell; (c) Stem; (d) Light impurities.

In a gas-solid two-phase flow system, the dynamic behavior of different components under the influence of airflow within the cleaning shoe creates a complex multicomponent coupled simulation scenario. To conduct simulations in EDEM, these components must be modeled as particles. Due to limitations in EDEM's modeling capabilities, only spherical particles can be created. Therefore, a particle packing method is used to simulate the shape of the actual components by combining multiple spherical particles. The models of the four component types are shown in Fig. 7.

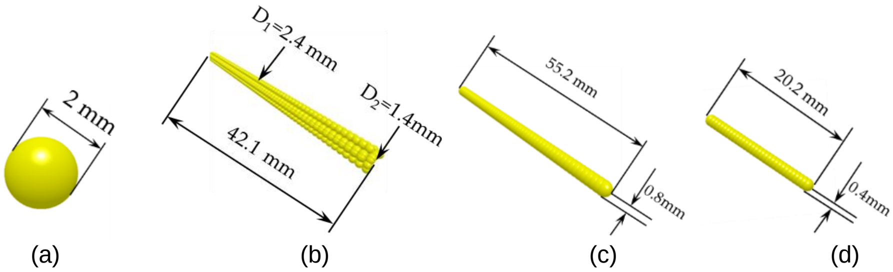

Fig. 7 - Particle filling model of the rapeseed threshed outputs
(a) Rapeseed; (b) Pod shell; (c) Stem; (d) Light impurities

The shape of the rapeseeds is approximated as spherical, so a single spherical particle can satisfy the requirements. The pod shell can be approximated as a semi-cylindrical hollow structure, while the stems and light impurities can be approximated as cylindrical.

In EDEM software, it is necessary to input the mechanical properties of the threshed output particles, as well as their contact coefficients with other objects. According to relevant references, the contact coefficients and mechanical property parameters for the threshed outputs are set as shown in Tables 2 and 3.

Particle Factory Settings. In EDEM software simulations, it is essential to define the distribution state of the threshed outputs within the cleaning shoe. To achieve this, the mass of each threshed output component was measured. The mass of threshed outputs collected in each receiving box was recorded (Fig. 5), and the overall three-dimensional distribution trend of the threshed outputs in the cleaning shoe was analyzed, as shown in Fig. 8(a). The proportion of each component was determined, with the results depicted in Fig. 8(b).

Table 2

Contact coefficients between different materials

Parameter	Restitution Coefficient	Static Friction Coefficient	Rolling Friction Coefficient	Parameter	Restitution Coefficient	Static Friction Coefficient	Rolling Friction Coefficient
Rapeseed - Rapeseed	0.19	0.81	0.05	Pod shell- Light impurities	0.08	0.63	0.02
Rapeseed - Pod shell	0.15	0.76	0.03	Pod shell- Cleaning sieve	0.10	0.61	0.01
Rapeseed - Stem	0.20	0.80	0.03	Stem-Stem	0.12	0.72	0.03
Rapeseed- Light impurities	0.15	0.76	0.03	Stem-Light impurities	0.12	0.75	0.03
Rapeseed - Cleaning sieve	0.52	0.45	0.01	Stem- Cleaning sieve	0.10	0.66	0.02
Pod shell - Pod shell	0.08	0.63	0.02	Light impurities - Light impurities	0.50	0.50	0.01
Pod shell - Stem	0.12	0.75	0.03	Light impurities- Cleaning sieve	0.10	0.61	0.01

Table 3

Material mechanical properties parameters

Parameter	Poisson's ratio	Density / kg m^{-3}	Elastic Modulus / MPa
Rapeseed	0.28	960	15
Pod shell	0.35	250	8
Stem	0.4	205	20
Light impurities	0.40	120	10
Cleaning sieve	0.33	7800	7100

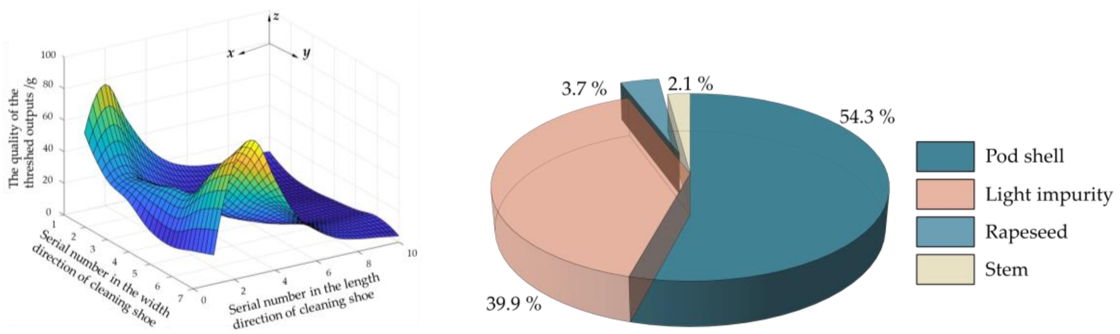

(a) (b)

Fig. 8 - Distribution of rapeseed threshed outputs under the threshing drum
(a) Distribution pattern of rapeseed threshing residue quality; (b) Proportion of threshed output components.

The cleaning efficiency and performance are directly related to the distribution of threshed outputs falling from the threshing device. To more accurately simulate real conditions, the generation and distribution of particles in the EDEM software are aligned with the actual distribution characteristics of the threshed outputs under the longitudinal axial flow threshing drum.

Based on the distribution patterns of the rape threshed outputs shown in Fig. 5 and Fig. 8 (b), three particle factory areas, slightly narrower than the width of the cleaning sieve and positioned 100 mm above the shaking plate, were established. These areas include a total of 13 particle factories, which are polygonal virtual regions in EDEM software used for particle generation. The total particle mass assigned to each particle factory corresponds to the mass distribution of threshed outputs shown in Fig. 8(a). The spatial distribution of the particle factory areas on the xy-plane is illustrated in Fig. 9.

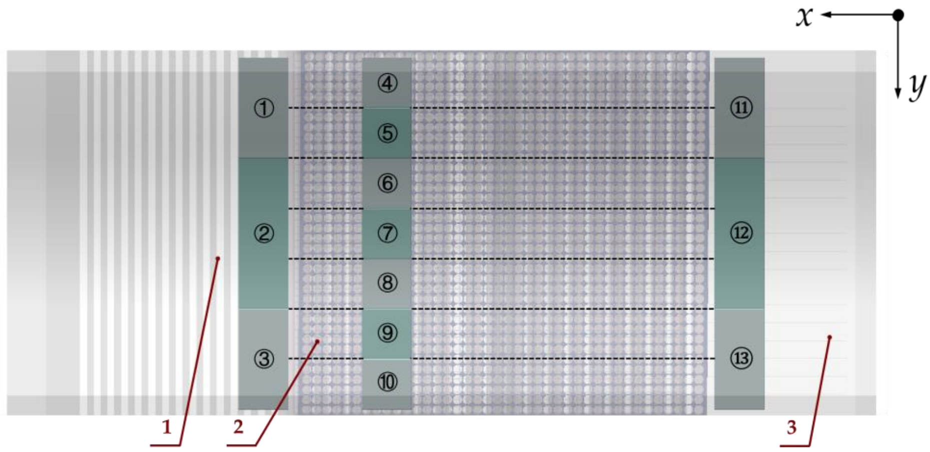

Fig. 9 - The particle factory distribution
1. Vibrating plate; 2. Perforated sieve; 3. Tail sieve

The first particle factory area is located above the tail of the vibrating plate, its length in the x direction is 110 mm, and the length in the y direction is 770 mm, and the ratio of 2:3:2 in the y direction is divided into three particle factories ①~③, which are mainly used to simulate the effect of the shaking plate in front of the threshing drum. The second particle factory area is positioned above the middle part of the perforated sieve, with a length of 110 mm in the x direction and 770 mm in the y direction. It is divided into seven particle factories (④~⑩) along the y direction. This area is situated in the region where the threshed outputs from the vertical axis flow threshing drum falls most densely and is primarily used to simulate the effect of the perforated sieve on the threshed outputs. The third particle factory area is located above the front part of the tail sieve, its length in the x direction is 110 mm, the length in the y direction is 770 mm, and the ratio of 2:3:2 in the y direction is divided into 3 particle factories ⑪~⑬, which is mainly used to simulate the effect of the tail sieve on the threshed outputs.

Based on experimental measurements, the ratio of input to threshed outputs in the cleaning shoe of the combine harvester is 9:4. Considering the proportions of each component in the threshed outputs shown in Fig.8(b), along with the density and moisture content of each component, the required number of particles for each particle factory can be calculated.

With the input rate of the combine harvester set at 3 kg·s-1, the differentiated settings of the particle factories allow for the creation of a distribution pattern in the cleaning shoe that is “more on the sides and less in the middle” along the y direction.

Coupling Simulation Settings. Import the MSH file format into Fluent to set up the numerical simulation parameters for the airflow phase. The standard κ-ε turbulence model was chosen to describe turbulent flow, and a pressure-based transient solver was employed. The environmental pressure was set to standard atmospheric pressure, and the direction of gravity acceleration was specified as the negative z-axis with a magnitude of 9.81 m·s^{-2}. Subsequently, the same MSH file was imported into EDEM for solid phase numerical simulation, with gravity acceleration also set as the negative z-axis, maintaining consistency. The boundary condition for the inlet was set as a velocity inlet, the airflow speed at inlet 1 was set to 17 m s^{-1}, and at inlet 2, it was set to 14 m·s^{-1}. The model's outlet was set as a pressure outlet with a relative pressure of 0 Pa. The vibrating sieve includes a shaking plate, a fish-scale sieve, a tail sieve, and a woven screen. The opening of the fish-scale sieve was set to 45°, with an x direction displacement of 6 mm, and a z direction displacement of 17 mm. The vibration frequency was set to 6.5 Hz.

User-defined function (UDF) was used to establish coupling between Fluent and EDEM, utilizing the Eulerian-Eulerian model for numerical simulation of the gas-solid two-phase flow. During the coupling process, the time steps were synchronized, Fluent’s time step was set to 5×10^{-5} s, and Rayleigh time step was set to 5×10^{-7} s. The total simulation duration was set to 1 s, with Fluent computational time being 100 times that of EDEM.

RESULTS AND DISCUSSION

Qualitative analysis of threshing outputs motion trends

The post-processing module in EDEM was used to export the movement trends of the particles. Distributions of the particles in the cleaning shoe at six representative time instances, 0.4 s, 0.6 s, 0.8 s, and 1 s, were selected to clearly observe the movement process of the particles, as shown in Fig. 10. Different colors were used to distinguish the components, black particles represent rapeseeds, green particles represent pod shells, yellow particles represent stems, and cyan particles represent light impurities.

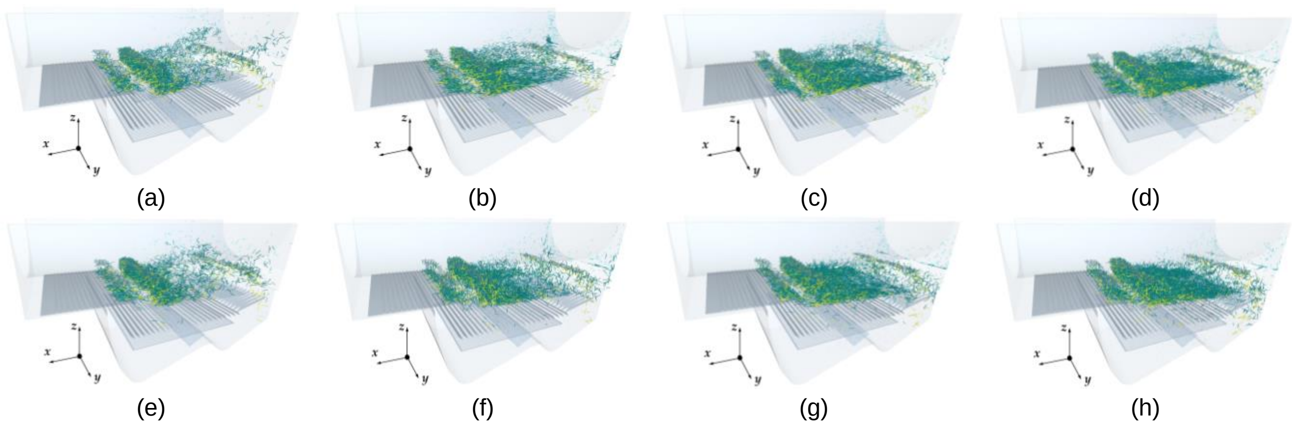

Fig. 10 - Distributions of the particles in the cleaning shoe

Figures (a), (b), (c) and (d) represent 0.4 s, 0.6 s, 0.8 s, and 1 s, respectively. The state of the cleaning sieve surface relative to the cleaning shoe is leaning forward and leaning right. Figures (e), (f), (g) and (h) represent 0.4 s, 0.6 s, 0.8 s, and 1 s, respectively. The state of the cleaning sieve surface relative to the cleaning shoe is horizontal.

In Fig. 10, these observations can be made, during the stage when the rapeseed threshed outputs fall from the particle factories to the perforated sieve (0~0.4 s), the particles of various components are influenced by the airflow from the fan's air duct, creating a waterfall-like descent. Rapeseed in both conditions begins to penetrate through the sieve, while threshed output components, excluding the rapeseeds, are driven by the airflow away from the sieve surface and towards the outside of the cleaning shoe. By this time, the threshed outputs passing through the perforated sieve is less than in the cleaning sieve horizontal condition.

In the period of 0.6~0.8 seconds, rapeseeds undergo further layering and sieving, with some rapeseeds having fallen onto the seed and impurities augers. In both conditions, along with rapeseeds falling through the perforated sieve, there are also impurities including pod shell, stem, light impurities.

By 0.8 seconds, the projectile motion trend of pod shells and light impurities gradually disappears. Pod shells that were suspended at relatively higher positions move to lower positions. At 1.0 second, the impurities particles above the perforated sieve move rapidly towards the outside of cleaning shoe in a flowing manner. The impurities exhibit a continuous outward movement trend. Additionally, there are more rapeseeds at the grain auger baffle in the cleaning sieve leaning forward and leaning right condition compared to the cleaning sieve horizontal condition.

Calculation of the rapeseed impurity rate and cleaning grain loss rate

After completing the numerical simulation, two key areas for counting the number of threshed output particles were defined in EDEM software, as shown in Fig. 11.

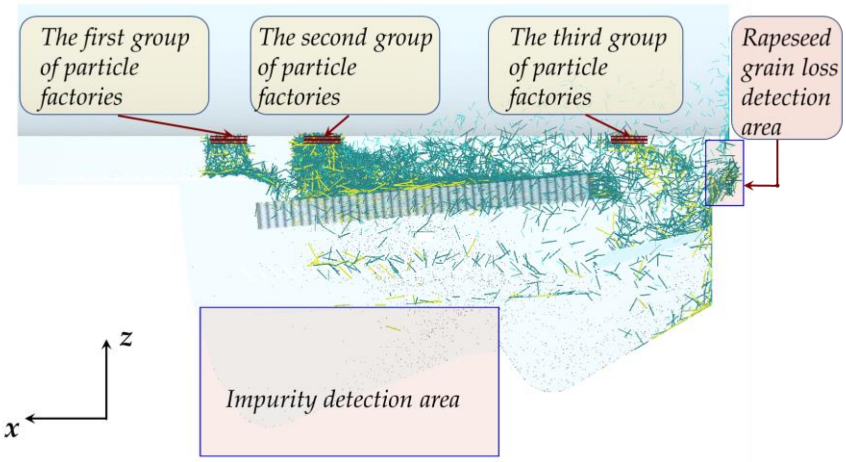

Fig. 11 - Schematic diagram of grain loss detection area and impurities detection area in the cleaning shoe

The first region is set near the grain auger and is used to count the number of rapeseeds, pod shells, stems and light impurities particles that pass through the cleaning sieve. This count is then used to calculate the impurity rate of the grains, which can be described by equation (7). The second statistical region is located at the outlet of the flow model and is intended to count the number of rapeseeds that are expelled from the cleaning shoe, thereby determining the cleaning loss rate. This rate can be calculated using equation (8).

$$P_1 = \frac{Q_1M_1 + Q_2M_2 + Q_3M_3}{Q_1M_1 + Q_2M_2 + Q_3M_3 + Q_4M_4} \cdot 100\% \tag{7}$$

where:

P_1 represents the impurity rate of the grains, %; Q_1 represents the number of pod shells that pass through the perforated sieve and vibrating sieve, pieces; Q_2 represents the number of stems that pass through the perforated sieve and vibrating sieve, pieces; Q_3 represents the number of light impurities that pass through the perforated sieve and vibrating sieve, pieces; Q_4 represents the number of rapeseeds that pass through the perforated sieve and vibrating sieve, pieces; M_1 represents the mass of a single pod shell, g; M_2 represents the mass of a single stem, g; M_3 represents the mass of a single piece of light impurities, g; M_4 represents the mass of a single rapeseed, g.

$$P_2 = \frac{Q_5}{Q_4 + Q_5} \cdot 100\% \tag{8}$$

where:

P_2 represents the cleaning loss rate, %; Q_5 represents the number of grains that are expelled from the cleaning shoe, pieces.

Based on equations (7) and (8), the grain impurity rate and cleaning loss rate for both cleaning conditions can be calculated. The combined evaluation metric, defined as cleaning performance, is determined by weighted summation. Given the practical requirements, the cleaning loss rate is generally considered slightly more important than the grain impurity rate. Therefore, the weight for the cleaning loss rate is set at 0.6, and the weight for the grain impurity rate is set at 0.4. A lower combined evaluation value indicates better cleaning performance. The calculation results are shown in Fig. 12.

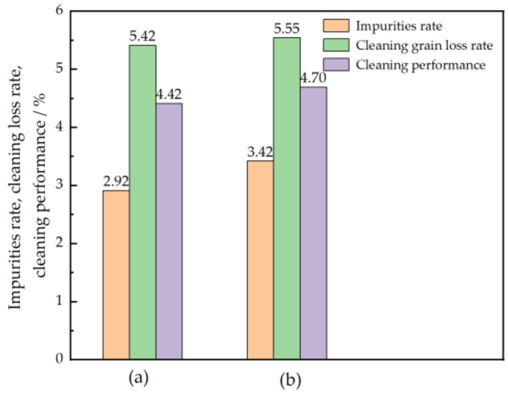

Fig. 12 - Comparison of cleaning performance

(a) The state of the cleaning sieve surface relative to the cleaning shoe is leaning forward and leaning right;
(b) The state of the cleaning sieve surface relative to the cleaning shoe is horizontal

The grain impurity rate and cleaning loss rate for the control group are 3.42% and 5.5%, respectively. In contrast, in the experiment group, the grain impurity rate and cleaning loss rate are 2.92% and 5.42%, respectively. Both values are lower than those for the horizontal position. Specifically, the grain impurity rate decreases by 14.6%, the cleaning loss rate decreases by 2.30%, and the overall cleaning performance metric decreases by 5.9% in the experiment group. This indicates that the sieve in the leaning forward and leaning right condition is more favorable for the cleaning of the threshed outputs.

Field experiment

To evaluate the operational performance of the multi-dimensional cleaning sieve, a harvesting operation was conducted in a hilly area where rapeseed is grown. Field experiments were carried out at the Longxin Agricultural Machinery Cooperative in 2023, f, Jiangxi Province. The selected rapeseed variety was Ganyouza 8, with a yield of 186 kg, an average plant height of 1480 mm, a pod height of 720 mm, a pod layer diameter of 460 mm, a thousand-seed weight of 3.86 g, and a seed moisture content of 17.3%. The field experiment is shown in Fig. 13.

Fig. 13 - Combine harvester harvesting rapeseed in hilly and mountainous areas

Before the experiment, a 25 m test field was measured, and markers were placed at both ends. The cutting width of the combine harvester was 2.0 m, with a stubble height of 700 mm and a forward speed of 1.0 m·s^{-1}. During the experiment, all material thrown out from the tail of the cleaning shoe was manually collected using mesh bag, rapeseed cleaning losses was manually separated from the tailings. The weight of the cleaning losses and the rapeseed grains in the grain tank was measured, and the impurity content in the grains was determined by sampling from the grain tank.

The rapeseed grain losses and impurity content under the conditions of the experimental group and the control group were compared, with each condition being repeated three times and the average value taken. The rapeseed grain loss and impurity content were calculated using the methods outlined in the Rapeseed Identification Guidelines. The cleaning loss rates for the experimental group and the control group were 1.41% and 2.03%, respectively, while the impurity contents were 2.18% and 2.64%, respectively. The experiment demonstrated that the rapeseed loss in the experimental group was reduced by 30.54% and 17.42%, proving that the designed multi-dimensional cleaning device effectively reduces field losses.

CONCLUSIONS

During the process of rapeseed harvesting in hilly and mountainous areas, terrain undulation and threshing device rotary operation lead to uneven threshed outputs distribution and on the sieve results in localized accumulation. This leads to poor airflow sieving efficiency and low cleaning efficiency in areas with higher threshed outputs concentration, while excessive airflow in areas with less threshed outputs causes grain-loss due to blowing rapeseeds out of the cleaning shoe. To address these issues, a multidimensional cleaning sieve design method is proposed. This method enables multi-degree adjustment within a limited space, enhancing both the uniformity of material distribution and the overall sieving efficiency.

The CFD-DEM gas-solid coupling approach was used to perform a detailed numerical simulation of a multi-degree-of-freedom cleaning device under specific feeding conditions. The grain impurity rate and grain loss rate were calculated for both the cleaning sieve leaning forward and leaning right condition (the experimental group) and the cleaning sieve horizontal condition (the control group). The comprehensive evaluation index of cleaning performance showed that, under the experimental group, the grain impurity rate decreased by 14.6% and the grain loss rate decreased by 2.3%.

This study not only deepens the understanding of the internal gas-solid two-phase flow characteristics within a multi-degree-of-freedom cleaning device but also provides important theoretical and technical support for improving the cleaning efficiency and operational performance of combine harvesters. By optimizing the sieve orientation, significant improvements in cleaning effectiveness can be achieved. Furthermore, this research provides a new measure to solve the problem of poor harvesting performance caused by the terrain of small harvesting machinery operating in hilly and mountainous areas.

ACKNOWLEDGEMENT

The work was supported by the National Natural Science Foundation of China (52405271), the Natural Science Foundation of Jiangsu Province (BK20230544) and the China Postdoctoral Science Foundation (310818).

REFERENCES

[1] Case IH Axial-Flow 9250. (2025). *Copyright©2025 CNH Industrial America LLC*. https://www.caseih.com/en-us/unitedstates/products/harvesting/axial-flow-250-series/axial-flow-9250
[2] Claas Lexion 8900. (2025). *All content©CLAAS KGaA mbH*. https://www.claas.co.uk/products/combines/lexion-8900-7400
[3] El-Emam, M.A., Zhou, L., Shi, W.D., & Han, C. (2021). True shape modeling of bio-particulate matter flow in an aero-cyclone separator using CFD-DEM simulation. *Computational Particle Mechanics, 8(4),* 955-971. https://doi.org/10.1007/s40571-020-00383-w
[4] Fendt IDEAL 10T. (2025). *News Archive*, *Copyright©AGCO GmbH*, 2019. https://www.fendt.com/us/combines/ideal-10t-highlights
[5] Li, Y.M., Liu, Y.B., Ji, K.Z., & Zhu, R.H. (2022). A fault diagnosis method for a differential inverse gearbox of a crawler combine harvester based on order analysis. *Agriculture-Basel, 12(9),* 1300. https://doi.org/10.3390/agriculture12091300
[6] Liu, Y.B., Li, Y.M., Dong, Y.H., Huang, M.S., Zhang, T., & Cheng, J.H. (2022). Development of a variable-diameter threshing drum for rice combine harvester using MBD-DEM coupling simulation. *Computers and Electronics in Agriculture, 196,* 106859. https://doi.org/10.1016/j.compag.2022.106859
[7] Li X., Zhao Y., Zhao H., LiS., Diao P. (2024). Design and testing of a gap adjustable elastic low damage corn picking header based on ADAMS, *INMATEH - Agricultural Engineering* 74(3), pp. 388-400, DOI: https://doi.org/10.35633/inmateh-74-34
[8] Ma, Z., Traore, S.N., Zhu, Y.L., Li, Y.M., Xu, L.Z., Lu, E., & Li, Y.F. (2022). DEM simulations and experiments investigating of grain tank discharge of a rice combine harvester. *Computers and Electronics in Agriculture, 198,* 107060. https://doi.org/10.1016/j.compag.2022.107060
[9] MF BETA 7370. (2025). *Copyright* © AGCO Corporation and its subsidiaries and affiliates. https://www.masseyferguson.com/en_gb/product/combine-harvesters/mf-beta.html#modal-brochure
[10] Shen, Z.H., Wang, W., Wang, G., Huang, D.R., & Jin, F. (2024). Interface velocity correction for improving resolved CFD-DEM simulation of two-phase flow in densely packed granular media. *Computers and Geotechnics, 174,* 106639. https://doi.org/10.1016/j.compgeo.2024.106639
[11] Tanneru, Y.S., Finke, J.H., Schilde, C., Harshe, Y.M., & Kwade, A. (2024). Coupled CFD-DEM simulation of pin-type wet stirred media mills using immersed boundary approach and hydrodynamic lubrication force. *Powder Technology, 444,* 120060. https://doi.org/10.1016/j.powtec.2024.120060

[12] Vlădut N.-V., Ungureanu N., Biris S.St., Voicea I., Nenciu F., Găgeanu I., Cujbescu D., Popa L.-D., Boruz S., Matei G., Ekielski A., Teliban G.C. (2023). Research on the identification of some optimal threshing and separation regimes in the axial flow apparatus, *Agriculture* 13(4): 838, DOI: 10.3390/Agriculture13040838, Agriculture-2301663
[13] Wang, H.Y., Huang, F.Y., Fazli, M., Kuang S.B., & Yu, A.B. (2024). CFD-DEM investigation of centrifugal slurry pump with polydisperse particle feeds. *Powder Technology, 447,* 120204. https://doi.org/10.1016/j.powtec.2024.120204
[14] Wang, L.J., Chai, J., Wang, H.S., & Wang, Y.S. (2021). Design and performance of a countersunk screen in a maize cleaning device. *Biosystems Engineering*, *209,* 300-314. https://doi.org/10.1016/J.BIOSYSTEMSENG.2021.07.008
[15] Xu, L.Z., Li, Y., Chai, X.Y., Wang, G.M., Liang, Z.W., Li, Y.M., & Li, B.J. (2020). Numerical simulation of gas-solid two-phase flow to predict the cleaning performance of rice combine harvesters. *Biosystems Engineering, 190,* 11-24. https://doi.org/10.1016/j.biosystemseng.2019.11.014tab
[16] Zhang J., Ding Y., Yang R., Pan Z., Mu J., Wang W., Liu Q, Wang S. (2024). Parameter calibration for discrete element simulation of cutting deck cleaning in small plot wheat combine harvester, *INMATEH - Agricultural Engineering* 72(1), pp.339-351, DOI: https://doi.org/10.35633/inmateh-72-31
[17] Zhang Z., Jiang H., He X., Zhang F., Wang J., Wang D. (2024). Design and test of threshing and cleaning device for Cyperus Esculentus L. combine harvester, *INMATEH - Agricultural Engineering* 72(1), pp. 798-808, DOI: https://doi.org/10.35633/inmateh-72-71
[18] Zhao Z., Yang X., Zhang G. (2022). Analysis and optimization test of operation process of cleaning device of corn seed harvester, *INMATEH - Agricultural Engineering* 68(3), pp. 211-220, DOI: https://doi.org/10.35633/inmateh-68-21